Improved Complete Ensemble Empirical Mode Decompositions with Adaptive Noise of Global, Hemispherical and Tropical Temperature Anomalies, 1850-2021

Charles David Coleman (chuckcoleman@yahoo.com)
US Census Bureau https://orcid.org/0000-0001-6940-8117

Research Article

Keywords: global warming, climate cycles, global warming acceleration, time series analysis, climate change, Hilbert-Huang transform

Posted Date: April 15th, 2022

DOI: https://doi.org/10.21203/rs.3.rs-1543477/v1

Improved Complete Ensemble Empirical Mode Decompositions with Adaptive Noise of Global, Hemispherical and Tropical Temperature Anomalies, 1850-2021

Charles D. Coleman
ORCID: https://orcid.org/0000-0001-6940-8117

Received: date / Accepted: date

Abstract ICEEMDAN, a variant of Empirical Mode Decomposition (EMD), is used to extract temperature cycles with periods from half a year to multiple decades from the HadCRUT5 global temperature anomaly data. The residual indicates an overall warming trend. The analysis is repeated for the Southern and Northern Hemispheres as well as the Tropics, defined as areas lying at or below 30 degrees of latitude. Multiannual cycles explain the apparently anomalous pause in global warming starting around 2000. The previously identified multidecadal cycle is found to be the most energetic and to account for recent global warming acceleration, beginning around 1993. This cycle's amplitude is found to be more variable than by previous work. Moreover, this variability varies by latitude. Sea ice loss acceleration is proposed as an explanation for global warming acceleration.

Keywords global warming · climate cycles · global warming acceleration · time series analysis · climate change · Hilbert-Huang transform

1 Introduction

Long-term variation in global temperatures is a well-known phenomenon. Improved Complete Ensemble Empirical Mode Decomposition with Adaptive Noise (ICEEMDAN, Colominas Schlotthauer and Torres 2014), a variant of the Empirical Mode Decomposition (EMD, Huang, Shen et al. 1998) decomposes time series of temperature anomalies into Intrinsic Mode Functions (IMFs) representing noise, cyles of different and possibly nonconstant frequencies and amplitudes and a residual. The last estimates the trend in temperature anomalies. Colominas, Schlotthaurer and Torres 2014 developed ICEEMDAN as an improvement

This article represents personal work by the author. Therefore, the U.S. Census Bureau can bear no responsibility for its contents.

C.D. Coleman
U.S. Census Bureau *Present address:* C.D. Coleman
5811 Governors View Ln.
Alexandria, VA 22310
USA
E-mail: chuckcoleman@yahoo.com

on prior EMD variants to more accurately reproduce the input signal and to reduce the remaining residual noise. They show that ICEEMDAN extracts signals more faithfully and with less residual noise than Ensemble Empirical Mode Decomposition (EEMD) (Wu and Huang 2009).[1]

The temperature anomaly data come from the Met Office Hadley Centre HadCRUT5 infilled observation datasets. (Dunn and Hogan in press) The data are for months between January, 1850 and December, 2019. For each 5° by 5° cell of the Earth's surface, the average temperature, 1961-1990, is computed. A monthly time series of temperature anomalies is constructed for each cell by subtracting the 1961-1990 average from the monthly estimated values. The averaged series are the averages of the anomalies for the area of interest, weighted by surface area. All available averaged series are used: global and Northern and Southern Hemispheres. In addition, a tabulation was obtained from the Met Office Hadley Centre for the Tropics, defined as latitudes between 30°N and 30°S. The mean for each series is used as the measure of temperature.

2 Previous Research

Previous research has followed four approaches. The first has concentrated on removing noise by smoothing data. The popularly displayed annual averages of Lindsey and Dahlman (2020) and others are simply the average of all months within a calendar year. Not only is the choice of periods to smooth is arbitrary, the smoothed data prevent identification of biennial, annual and subannual cycles. Moreover, identification of multiannual data is hampered by preventing the contributions of individual months from being identified. Variations in the timing of cycles with periods of a few years can result in their nonidentification. Hansen et al. (2006) avoided this by focusing on the changes over time and not attempting any decompositions or forecasts. Hansen, Sato and Ruedy (2013) similarly use annual averages in an analysis of climatic forcing. Hansen and Sato (2021) use a linear trend to identify putative recent global warming acceleration. A 21-year weighted moving average has happily been discontinued from the Internet.

The second approach is regression analysis. Foster and Rahmstorf (2011) and Zhou and Tung (2013) use linear regression on global data to obtain linear trends after controlling for forcing variables. The obvious criticisms are that the trends are not necessarily linear, the forcing variables may not have linear effects, missing variables may be present and that the time series structure is not used in any way. Lean and Rind (2008) partition the Earth's surface into cells, then run regressions within each cell and combine results. This approach suffers from not explicitly incorporating the spatial structure in what is really a spatial panel model. An additional weakness of regression is that statistical significance does not imply practical significance (Ziliak and McCloskey 2004; McCloskey and Ziliak 2008). When a variable lacks practical significance, controlling for it has no practical effect on regression fit. Turner, Colwell et al. (2005) use regression analysis on monthly Antarctic temperature and wind speed data to obtain linear trends. This approach has the defects of assuming linearity and not accounting for time series structure. Thus, their results suffer from bias and, at best, can only be interpreted qualitatively.

The third approach uses wavelet analysis. A full description of wavelet analysis is beyond the scope of the present paper. A short description is that a basis function is chosen

[1] Torres, Colominas and Schlotthauer 2014, Figure 2, does not display ICEEMDAN's two residual IMFs for that example while displaying all five of EEMD's residual IMFs.

that, in turn, generates other basis functions that are used to form a wavelet representation of a signal. The exact representation depends on the choice of initial basis function. Recovering amplitude and frequency information is mathematically complicated. Lau and Weng (1999), Silva, Silva et al. (2018) and Yang, Wang et al. (2015) are examples of applying wavelet analysis to monthly temperature data. The starting dates of these analyses, 1884 (Silva, Silva et al. 2018) and 1955 (Lau and Weng 1999; Yang, Wang et al. 2015), show an important limitation: these analyses do not use the full time series because of the initial noise, as decribed in Section 4. Moreover, the trends are linear, a constraint that EMD lacks.

Empirical Orthogonal Functions (EOFs) appear to have fallen out of favor in climatic research. EOFs are the principal components of spatiotemporal data (Björnsson and Venegas 2000). The components are called "modes of variability," Their problem lies in their being "primarily *data modes, and not necessarily* physical modes" (Björnsson and Venegas 2000, p. 5, original emphasis). Without physical knowledge, they provide little information about physical phenomena. Examples of their application to climatic data, including global warming, include Björnsson and Venegas (2000), Bretherton, Widman et al. (1999), Feldstein (2002) and Wang and Mehta (2008).

The last approach uses the data-driven Empirical Mode Decomposition (EMD) or Ensemble Empirical Mode Decomposition (EEMD) (Wu and Huang 2009) and seems to be the most popular recently. Section 3 delves into the technical details. Huang, Wu et al. (2009) appear to have been the first. They use EMD to remove noise from monthly global temperature anomaly series to derive annual series. Wu, Huang et al. (2011) essentially repeat the analysis using EEMD and identify a nearly regular multidecadal cycle. Franzke (2010) uses EEMD to remove noise from Antarctic temperature series to identify trends. Shi, Yang et al. (2011) and Xing, Chen et al. (2016) apply EEMD to tree ring records. Qian (2015) uses EEMD to remove noise from Shanghai, China temperature extreme series to identify the effects of urbanization on them. Yang, Wu and Hu (2011) apply EMD to air temperature observations at Nanjing, China to find no detectable solar-driven variability, which the present paper confirms globally. Mukherjee, Joshi et al. (2014) apply EEMD to daily Indian monsoon rain totals. Similarly, Sabzehee, Nafisi et al. (2019) analyze Caspian Sea catchment rain totals.

3 Empirical Mode Decomposition

Huang, Shen et al. (1998) introduced the Empirical Mode Decomposition (EMD) as an adaptive, data-driven method to completely decompose time series using the Hilbert Transform. The Hilbert Transform is a more general version of the Fourier Transform, decomposing a time series into the sum of series of the form

$$\phi_j(t) = a_j(t)\sin(\omega_j(t)t + \theta_j(t)) \tag{1}$$

where a_j is the amplitude of ϕ_j, ω_j is its possibly time-varying period and θ_j is its possibly time-varying phase shift. The true ϕ_j are the modes of the input signal. The estimates $\hat{\phi}_j$ are Intrinsic Mode Functions (IMFs) which should satisfy the condition that the number of extrema should differ from the number of zero-crossings by 0 or 1. Given a residue r_j, with r_0, the initial residue equal to the input signal, EMD proceeds to sift r_j to produce IMF^{j+1} and r_{j+1} by first constructing upper and lower envelopes by interpolating the local maxima and minima, respectively, then subtracting their local means from r_j to obtain h_j. If h_j is an IMF, then it is output as IMF^{j+1} and r_{j+1} is set equal to $r_j - h_j$. Otherwise, the algorithm repeats, using r_{j+1} and iterated until an IMF is produced or a stopping criterion is reached,

in which case a defective IMF is output. IMFs are subsequently output until r_j has 2 or 3 extrema, in which case it is output as the residual trend. EMD ideally outputs IMFs in order of increasing period or, equivalently, decreasing frequency.

EMD is well-known for mode-mixing (outputting a single IMF for multiple ϕ_j), mode-splitting (outputting multiple IMFs for a single ϕ_j) and producing spurious IMFs. Several methods have been developed to remedy this, including EEMD, CEEMDAN (Schlotthauer, Colominas et al. 2011), ICEEMDAN and MAEMD (Deering and Kaiser 2005). These methods are all ensemble methods that add a function to multiple copies of the input, then average the outputs. This enables them to reduce EMD's mode-mixing and mode-splitting (Huang, Shen et al. 1998). The first two add white noise, ICEEMDAN adds IMFs derived from white noise and MAEMD adds and subtracts a masking sinusoid. All average the results of their decompositions. Ensemble methods have the further advantage of being able to separate the noise which EMD lacks (Kim, Kim and Oh 2012). Ensemble methods are not guaranteed to produce proper IMFs because the average of IMFs is not necessarily an IMF (Steven Sandoval personal communication). All EMD methods are subject to outputting residual IMFs due to possible nonorthogonality of the IMFs that represent the input signal The summed IMFs are subtracted from the temperature anomaly input to obtain the temperature trend, with the obvious interpretation. Colominas et al. (2014) showed that ICEEMDAN outputs IMFs in decreasing order of frequency with fewer residual IMFs than EMD, EEMD and CEEMDAN and does not output residual IMFs before outputting all informative IMFs. ICEEMDAN is run with 10,000 ensemble members and the default SNR of 0.2. The number of ensemble members was empirically determined to provide stable decompositions. The number of IMFs was set to 8 to avoid residual IMFs and to include a residual ninth IMF in the residual trend.

EMD has the further advantage of being applicable to any type of time series. Fourier series have the tightest restrictions: linearity and stationarity. Wavelets permit nonstationarity but require linearity. Fourier series and wavelets require a priori bases, while EMD is adaptive. EMD is chosen to minimize assumptions.

4 Results

This Section presents selected graphs illustrating the termperature anomaly decompositions and provides some interpretations . The decompositions were performed for all downloaded series. R (2020) codes, an R workspace and undisplayed graphs are in the Supplemental materials. Additionally, for each decomposition, the Hilbert spectrum, the time-frequency-amplitude spectrum associated with each IMF^j, $H_j(\omega,t)$, is defined as

$$H_j(\omega,t) = \begin{cases} a_j(t), & \omega = \omega_j \\ 0, & \text{otherwise} \end{cases}. \tag{2}$$

Frequencies and amplitudes are displayed separately. Negative frequencies appear occasionally as a result of a violation of the IMF condition. For example, a trough may occur at the expected time but not cross zero (that is, remain positive). In the absence of a well-founded interpretation, these should be ignored. They are only reported for completeness. As necessary, the Marginal Hilbert Spectrum for an IMF is calculated as

$$h_j(\omega) = \frac{1}{T}\int_{1850:1}^{2021:12} H_j(\omega,t)dt$$

$$\approx \frac{1}{172 \times 12} \sum_{t=1850:1}^{2021:12} a_j(t) I(\omega = \omega_j(t)), \tag{3}$$

where I is the indicator function and the limits have the format year:numeric month. The final, presented $\tilde{h}_j(\omega)$ is then obtained by applying the Epannechnikov kernel smoother to $h_j(\omega)$ for all $\omega > 0$. The smoothing turns the discontinuous $h_j(\omega)$ into a continuous, more interpretable function. The final result displays amplitude as a function of frequency, similar to a Fourier Spectrum. Only the modes are analyzed, as they are invariant to expression by frequency or period, unlike averages. They also have the interpretation of being spectral peaks.

A final concept used is the energy or power of a signal. For a signal y_t, its energy is the integral of its squared amplitude:

$$e(y) = \frac{1}{T} \int_t a_t^2(t) dt, \tag{4}$$

where T is the length of y_t. Since an IMF is centered, its energy is equal to its variance.

A full analysis is provided only for the global data. Decompositions and trend analyses only are provided for the other datasets.

4.1 Decompositions

Figure 1 displays the global median temperature anomaly for 1850-2021. Several things are readily apparent. Average temperature is rising throughout the period, with sustained declines during the approximate periods 1880-1910, 1940-1970 and 2000-2010. The series is particularly noisy before 1900. The reduction of noise over time, especially during the satellite era, reflects better measurements.

4.1.1 Global

Figure 2 displays the ICEEMDAN decomposition of median global termperature anomalies. IMF 1 estimates the noise. IMFs 2-8 estimate the respective ϕ_j, in descending order of frequency. IMF 1's amplitude is particularly high before around 1890. Figure 3 shows that IMF 1's amplitude rose to a sustained peak around the 1870s. The additional noise in IMF 1 spills over into the other IMFs, especially IMFs 2 and 3, which show amplitude peaks coinciding with IMF 1's early peak. Figure 4 displays the frequencies. IMF 1 is clearly the noise mode with its greatest variation in frequency, ranging from near 0 to near 6, the Nyquist frequency. IMFs 2 and 3 show clustering around 2 and 1 cycle(s) per year: these are the semiannual and annual IMFs. IMFs 4-8 have frequencies of less than 1 per year.

To better understand the frequencies, Figure 5 shows the periods: the reciprocals of the frequencies. IMF 4 is dominated by 2 year periods. IMF 5's period fluctuates between 1 and over 20 years. IMF 6 shows a peak period of over 3300 years in 2008 in the middle of a surge from 2006 to 2011. This correspondes to a period of slowing, than decreasing decline in IMF 6. IMF 7's period generally varies between 10 and 20 with increases to around 60 years and declines below 5 years. IMF 8's period generally lies between 50 and 90 years, with an increase to almost 500 in 1992. While the subsequent decline is largely explained by global warming acceleration, discussed below, its onset before acceleration is difficult to understand.

Figure 6 shows the smoothed Marginal Hilbert Spectra for IMFs 5-8. While this Figure confirms that frequencies are decreasing, it is otherwise hard to interpret. Figure 7 displays the inverted Marginal Hilbert Spectra. The horizontal axis has the natural interpretation of being the period. IMF 5 shows a modal period of 7 years, with a positively skewed spread of 3-17 years. IMF 6's mode is 9 years, with a wider, similarly skewed spread of 7-25 years. Its uppermost year is well to the right. IMF 7 shows the most variability, with its main mode at 16-17 years, a nearly equal mode at 22 years, a major secondary mode at 37 years and a minor mode at . IMF 7's upper tail does not decay to 0 by 50 years. In fact, it remains relatively high. IMF 8's period peaks at 71 years, with a small skewness of -0.13 for the periods displayed. No IMF corresponds to the 11-year solar cycle. Its energy is too low to distinguish it from the noise. Table 1 shows that the multidecadal IMF 8 has the greatest energy. This, and its timing, is consistent with Wu, Huang et al. (2011) with the exception that its amplitude is even more variable. Moreover, IMF 8 accelerates beginning in 1993, which will be explored more in Subsection 4.2.

4.1.2 Regional

Figures 8, 9 and 10 display the monthly average temperature anomalies and their decompositions for the Northern Hemisphere, Southern Hemisphere and Tropics, respectively. With the exception of IMF 8's amplitudes, as explained in Subsubsection 4.2, they are generally similar. Table 2 shows the trend increases in the temperature anomalies, globally and regionally. It shows two effects. First, warming is greater at higher latitudes as shown by the greater temperature increase globally compared to the Tropics when they have approximately the same share of land area: 29.2% globally and 28.6% in the Tropics.[2] Excluding ice-covered surfaces from the calculation only increases this effect. Second, greater surface land area increases warming. Land covers 29.3% of the Northern Hemisphere compared to 19.1% of the Southern Hemisphere. Again, excluding ice-covered surfaces increases this latter effect.

4.2 Global Warming Acceleration and Hiatus

By decomposing temperatures into their constituent modes we can obtain insights into observed phenomena and new phenomena. The most important is a fuller explanation of Hansen and Oh's (2021) finding of recent global warming acceleration. We find that this warming begain around 1993, which is not apparent from their graphs that show a recent, possibly temporary, increase above above a linear trend. We posit that accelerating sea ice decline is the cause of global warming acceleration. We also find that the Global Warming Hiatus that first appeared in the media and Internet (Easterling and Wehner 2009) and was subsequently analyzed by many is at least mostly a mirage caused by the confluence of multiannual cycles.

Figure 11 displays IMF 8 globally and for each region studied. Close examination shows a recent acceleration in the global cycle, which is harder to discern regionally. Figure 12 shows the derivative of each corresponding IMF 8 with respect to time. In each geography, IMF 8 is sinusoidal with varying amplitudes and a 50-year period. However, the first peak corresponds to a flatter, declining period in the Tropics. The derivative of global IMF 8 presents a point of inflection in 1993, which leads to a slowing of the rate of temperature increase, then accelerating increase. The regional graphs are more subtle. Each derivative of

[2] I'd like to thank D.W. Rowlands for calculating the latter figure.

IMF 8 is sinusoidal (except, of course, the Tropics before around 1900) until 1993 when, outside of the Southern Hemisphere, they turn into roughly straight lines above the expected continuations of the sinusoids. The Northern Hemisphere has an accelerating temperature increase, while the Tropics has a decelerating decrease. These are all equivalent to, and contributing to global temperature warming acceleration. The weakness or absence of the acceleration in the Southern Hemisphere may indicate more specifically that it is the decline in Northern sea ice that is driving acceleration. Hansen and Oh (2021) extrapolate a linear approximation of a 132 running mean of global temperatures, 1970-2015, to find that temperatures afterwards are above expectation. They conclude that global warming acceleration began in 2015 based on Loeb, Johnson et al.'s (2021) interpretation of CERES (Clouds and the Earth's Radiant Energy System) satellite data. Instead, we propose that increasing loss of sea ice has been causing global warming acceleration. Sea ice is an excellent candidate because ice reflects more sunlight than seawater. Thus, its loss increases global warming. beyond that caused by any other forcings (Dai, Luo et al. 2019). According to National Snow and Ice Data Center (2020) Figure "Mean sea ice anomalies, 1953-2018," Northern Hemispheric sea ice started declining around 1988 with evidence of acceleration.

Figure 13 shows the sum of the multiannual median IMFs 5-8, and residual trend. The cooling period during the 2000s now appears. It is clear that this global waming hiatus, originally analyzed by Easterling and Wehner (2009), occurred as a result of the multiannual cycles corresponding to IMFs 5-7 being in declining phases, even while IMF 8, the most energetic IMF, was increasing. When these cycles resumed increasing, the cooling period ended. IMF 7 peaks around 2000, though it alone is not enough to account for the pause due to its low amplitude.

5 Discussion

We have used ICEEMDAN to decompose the Met Office Hadley Centre's median monthly temperature anomaly into noise, cycles and a residual trend. Our most important finding is global warming acceleration beginning around 1993,[3] The global cooling hiatus of the early 2000s is coincidental, being the result of cyclic downturns.

The multidecal cycle with a period of 50 years is responsible for global warming acceleration. We hypothesize that this is due to accelerating sea ice loss, which is documented to have begun around 1988, two decades earlier than the start of Hansen and Sato's (2021) claim. This is supported by Hugonnet, McNabb et al. (2021), who find that global glacier ice mass loss has been accelerating during 2000-2019, providing confirmation of global warming acceleration during this period.[4] These three accelerations suggest some sort of linkage. Hu Hansen and Sato (2021) use linear regression to produce a smooth trend for the global average temperature anomaly, 1970-2015.[5] This is based on the 132 month running mean, which appears close to linear, during 1970-2015. They then find that the global temperature anomaly after 2015 is completely above this trend. They hypothesize that this is due to increased atmospheric aerosols increasing temperature forcing, leading to accelerated global warming. However, lacking information about temperature cycles, they cannot determine whether they are truly observing acceleration, a temporary or permanent change in trend or an anticipable peak in an underlying cycle. Their inability to precisely identify whatever they

[3] Due to estimation error, the precise timing in unavailable. Fortunately, this error is in the range of months.

[4] Glacier ice mass loss is linearly proportionate to local temperature increase (Hugonnet, McNabb et al. 2021). Accelerating loss can only be caused by accelerating increase.

[5] Unfortunately, Hansen and Sato (2021) do not cite their data source.

found precludes policy prescriptions. Instead, our evidence provides actionable information: Sea ice restoration should be a part of global warming mitigation. IMF 8's early Tropical nonappearance and early weak appearance at other latitudes is worthy of investigation.

The global cooling pause has a simple explanation in decreases in global multiannual cycles, which can be seen individually in Figure 2. IMFs 5-8 and in their sum including the residual trend in Figure 13. Each of these IMFs has a particularly low trough after 2000, consistent with a negative forcing. Ridley, Solomon et al. (2014) provide evidence for this forcing in the form of increased and variable stratospheric volcanic aerosols. Coincidence with a modal trough can lower that trough. Militating against this is the accelerating global glacier ice loss during this period. The increased CO_2 uptake of Keenan, Prentice et al. (2016) and the similar increased photosythesis hypothesis of Leggett and Ball (2015) have to be rejected because these would have been reflected in sustained decreases in low frequency IMFs in the ICEEMDAN decompositions.

The first three cycles have clear physical intepretations. The semiannual and annual cycles (IMFs 2 and 3) capture the seasonal variations in average temperature driven by changes in absorbed insolation. The biennual cycle reflects the Quasi-Biennial Oscillation possibly interacted with other phenomena with approximately biennal cycles.

Pooling observations, in this case, 5° by 5° latitude-longitude cells, reduces the relative noise, thus increasing identifiability of cycles and trends. As is visible in the early decades of the series, noise can spillover into low frequency cycles. As the noise increases, increasingly lower frequency cycles can become unidentifiable. Moreover, except for the very lowest frequency cycle, the lowest frequencies have the least energy per Table 1. Their low energies are additional impediments to their identification in the presence of noise. Thus, EMD and its derivatives have to be used on temperature series that have pooled enough observations to reduce noise to a manageable level. It may be possible to use a spatiotemporal generalization of EMD on a grid, provided that the spatial structure enables canceling enough noise to improve identifiability. Coarser grids may accomplish this at the potential risk of producing too little spatial detail. An improved version of the spatial EMD of Fauchereau, Pegram, and Sinclair (2008) may be able to do this. A requirement is the ability to draw strength across space to reduce noise.

6 Conclusions and Extensions

Understanding multiannual temperature cycles can shed new light on the climate in general. The global warming acceleration that began in 1993 is only visible in the multidecadal cycle. This acceleration is proposed to be due to accelerating sea ice loss beginning around 1988, particularly in the Northern Hemisphere. This improves on Hansen and Sato's (2021) claimed recent global warming acceleration based on extrapolating a trend. By using cyclical information, we have avoided the biases from not accounting for cyclical information when forecasting. Moreover, we have pinpointed, within estimation variation, the beginning of this acceleration. The strongest evidence of global warming acceleration lies in accelerating global glacial ice mass loss during 2000-2019. Confirmatory research is needed to verify that sea ice loss has indeed been accelerating and to fully incorporate Southern Hemispheric sea ice loss into explanations of global temperature warming acceleration. The policy implication is clear: sea ice restoration is a necessary part of global warming mitigation.

The Global Warming Hiatus has been shown to be, at most, the effect of volcanic forcings. It may very well have been a mirage. Again, this was only made possible by decomposing global termperature changes into their underlying trend and cycles. The Hiatus had

Table 1 IMF Energies

IMF	Energy * 1000
1	3.8
2	2.1
3	2.3
4	2.9
5	2.6
6	2.2
7	1.4
8	8.0

Table 2 Temperature Anomaly Residual Trend Changes

Region	Degrees Celsius
Global	0.76
Northern Hemisphere	0.92
Southern Hemisphere	0.58
Tropics	0.62

minimal, if any, effect on global glacial ice mass loss. Accelerating global glacial ice loss provides evidence against the hiatus.

ICEEMDAN, the technique we used, is superior to EMD and EEMD, the previous EMD-based methods to analyze global temperature changes due to its abiity to handle noise, output informative IMFs in decreasing order of frequency and reduction of residual IMFs. All of these techniques share the advantages of being data-driven, having minimal assumptions and being applicable to almost any kind of time series. In particular, they do not require assuming particular functional forms for the cycles or trends. They can be used to improve climate models by identifying temperature and other cycles with variable amplitudes and frequencies. Even the estimated noise can inform these models. It may be possible to develop a spatial method that accounts for spatial correlations and draws strength across space to provide local EMD-style decompositions.[6] These can provide local information to better improve climatic understanding and inform climate models.

Acknowledgements I'd like to thank D.W. Rowlands for calculating the Tropical surface water percentage, the Met Office Hadley Centre for providing me with the Tropical data series and an anonymous referee for helpful comments.

Availability of data and material

Global and hemispheric source data are from the Met Office Hadley Centre observations datasets at https://www.metoffice.gov.uk/hadobs/hadcrut5/data/current/download.html, downloaded February 17, 2022. Tropical data are from a file emailed by the Met Office Hadley Centre on the same date. All data are included in the supplemental materials.

[6] Fauchereau, Pegram, and Sinclair (2008) is a first step in this direction.

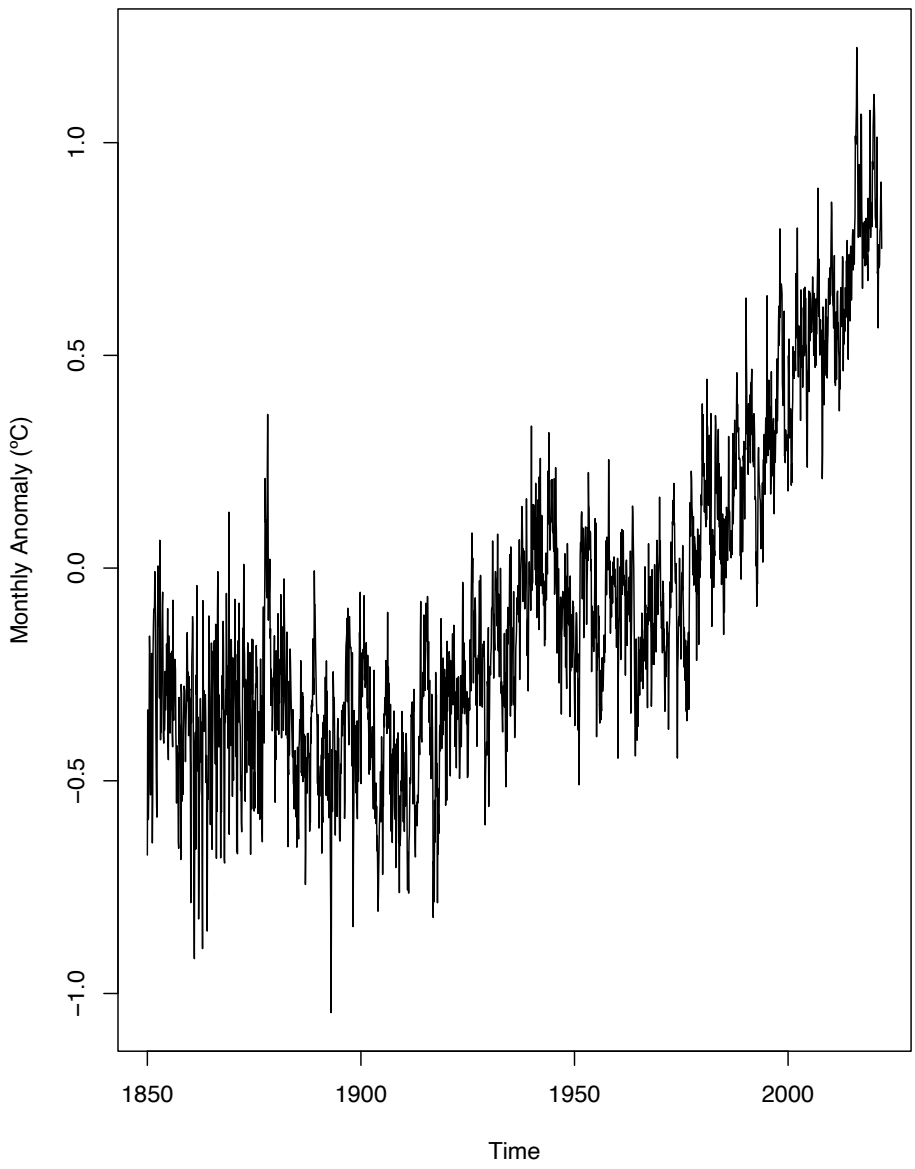

Fig. 1 Mean Average Global Temperature Anomalies, 1850-2021

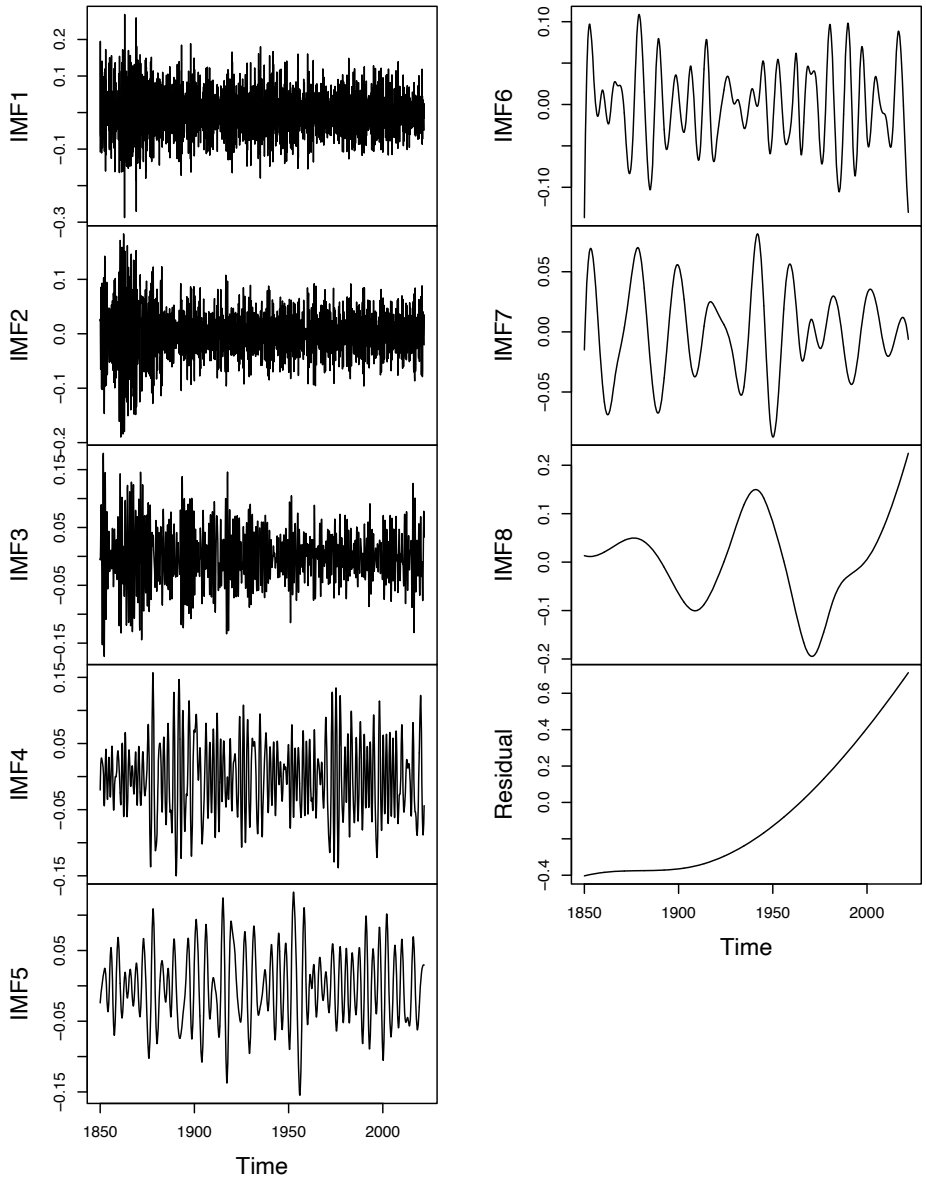

Fig. 2 ICEEMDAN Decomposition of Mean Average Global Temperature Anomalies (°C), 1850-2021

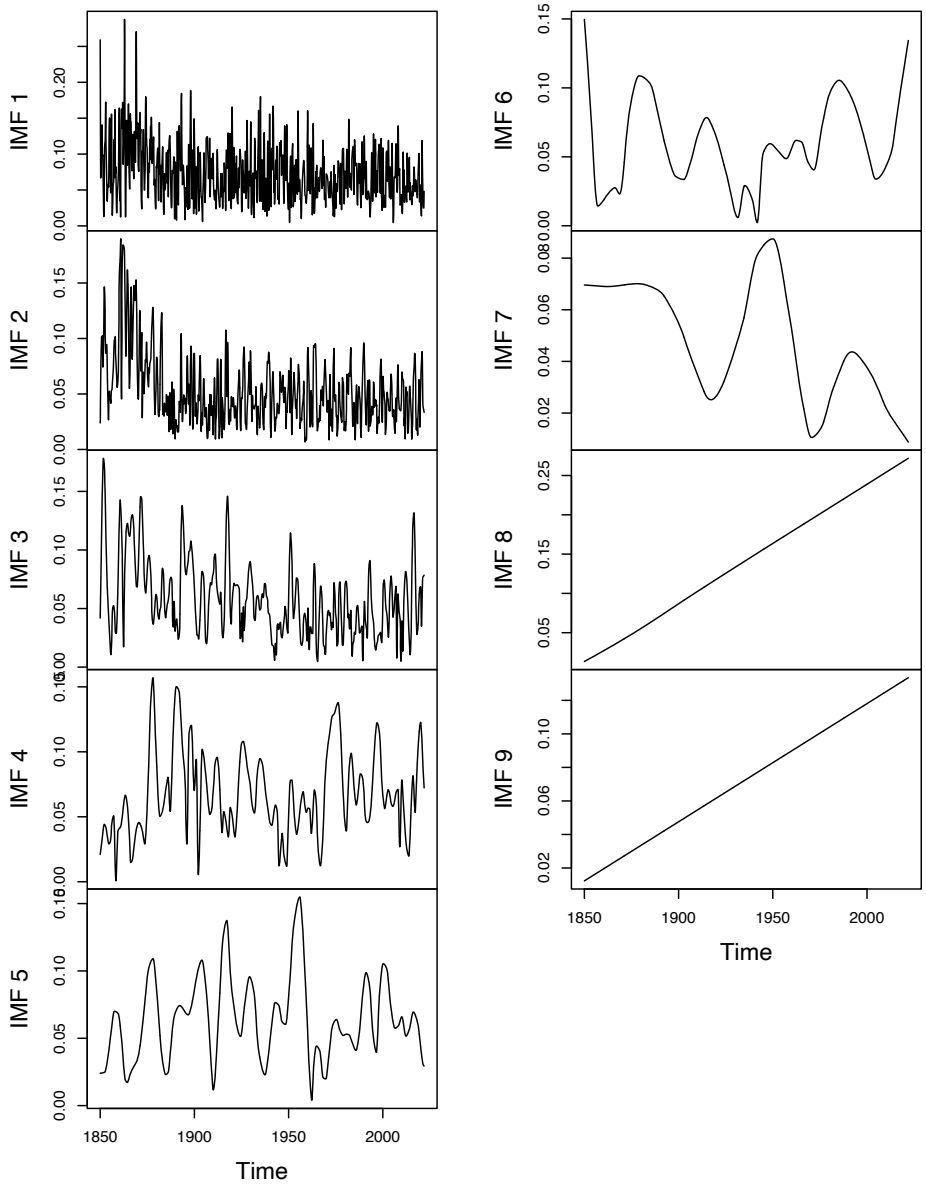

Fig. 3 Amplitudes of Mean Average Global Temperature Anomalies IMFs (°C), 1850-2021

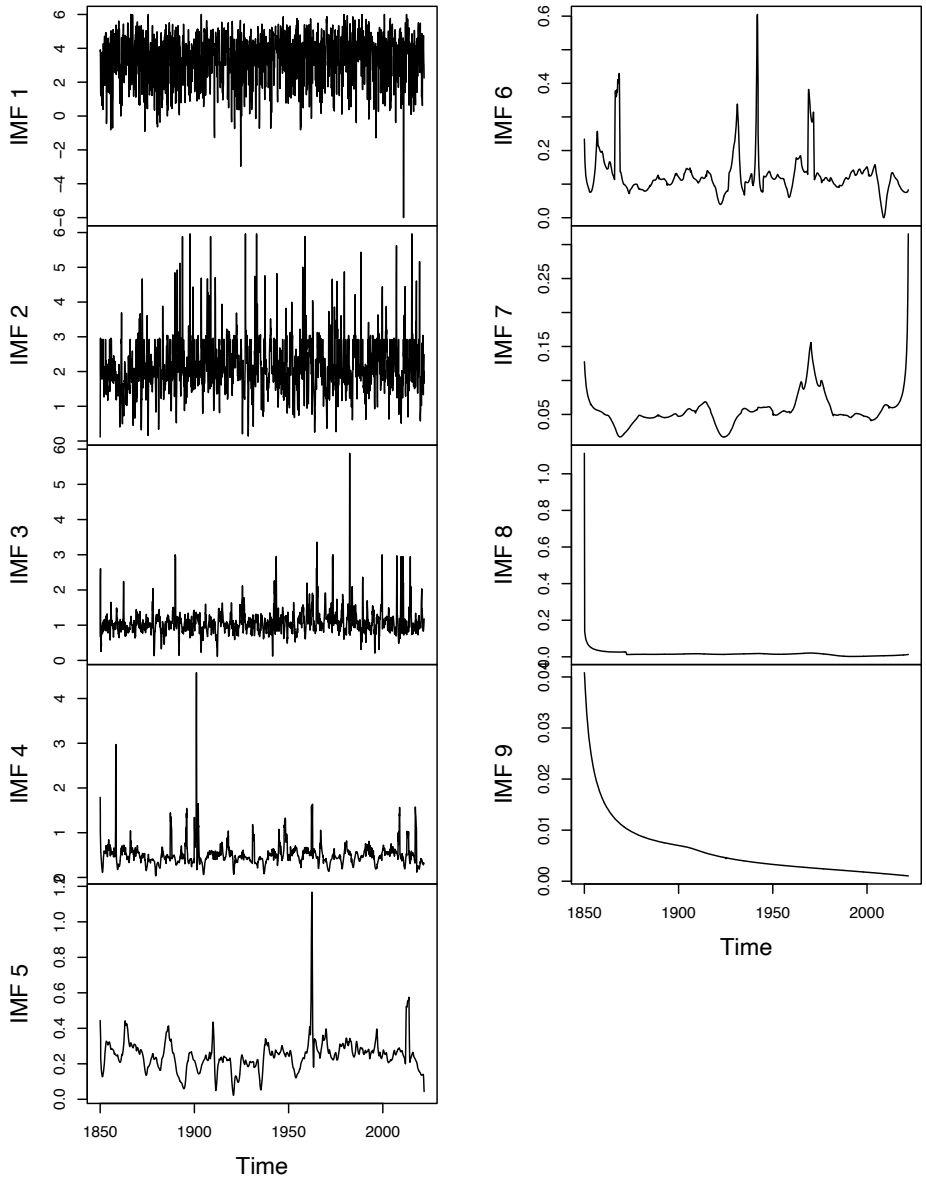

Fig. 4 Frequencies of Mean Average Global Temperature Anomalies IMFs (cycles/year), 1850-2021

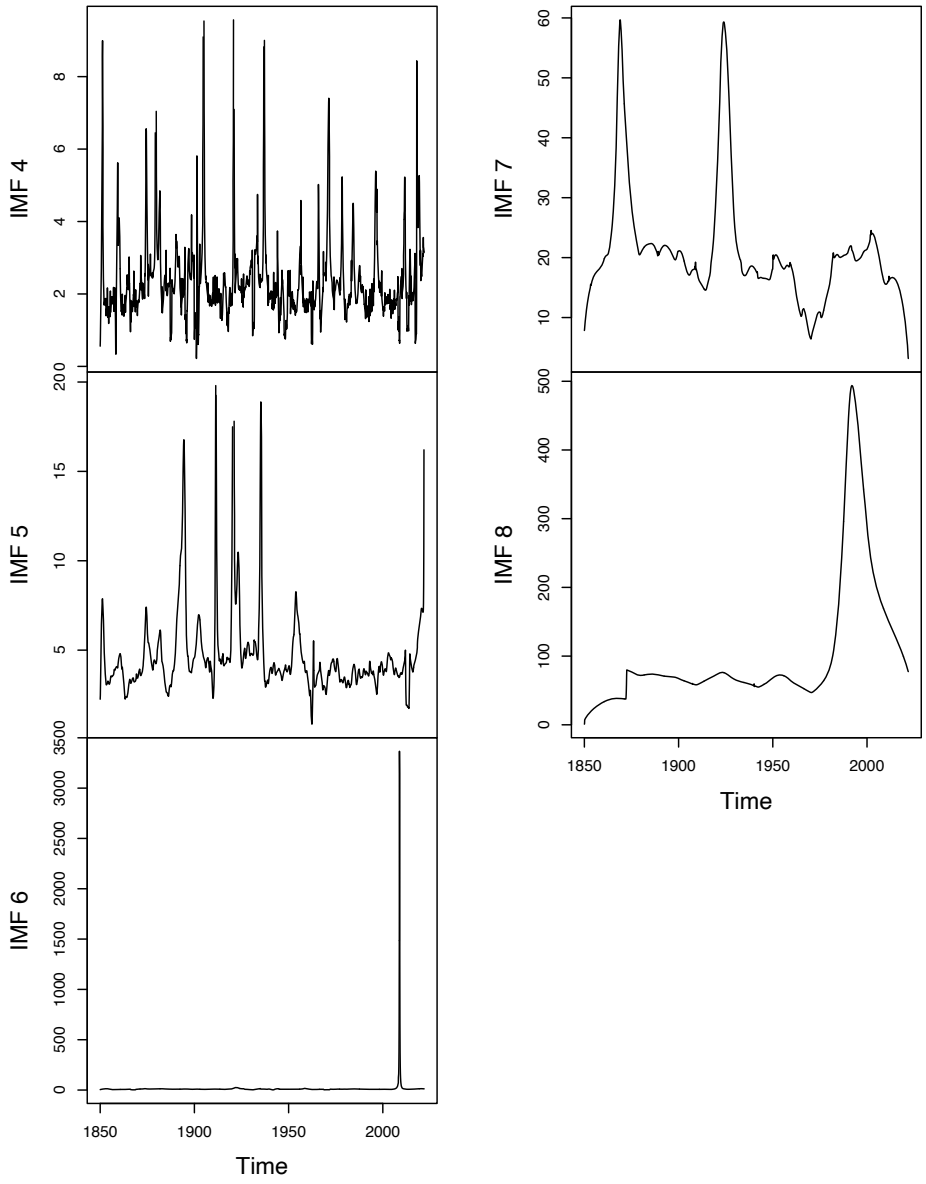

Fig. 5 Periods of Mean Average Global Temperature Anomalies, IMFs 4-8 (years), 1850-2021

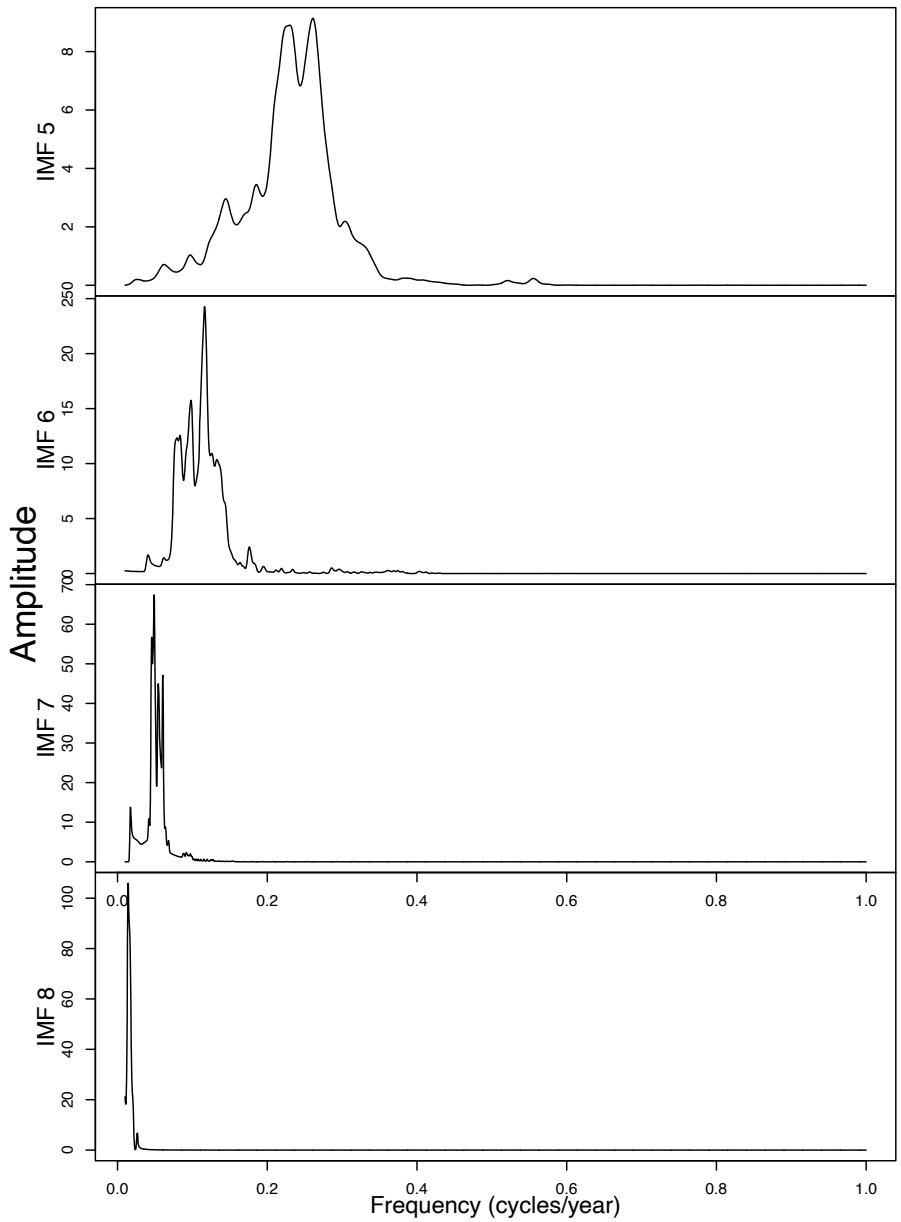

Fig. 6 Marginal Hilbert Spectra, IMFs 5-8

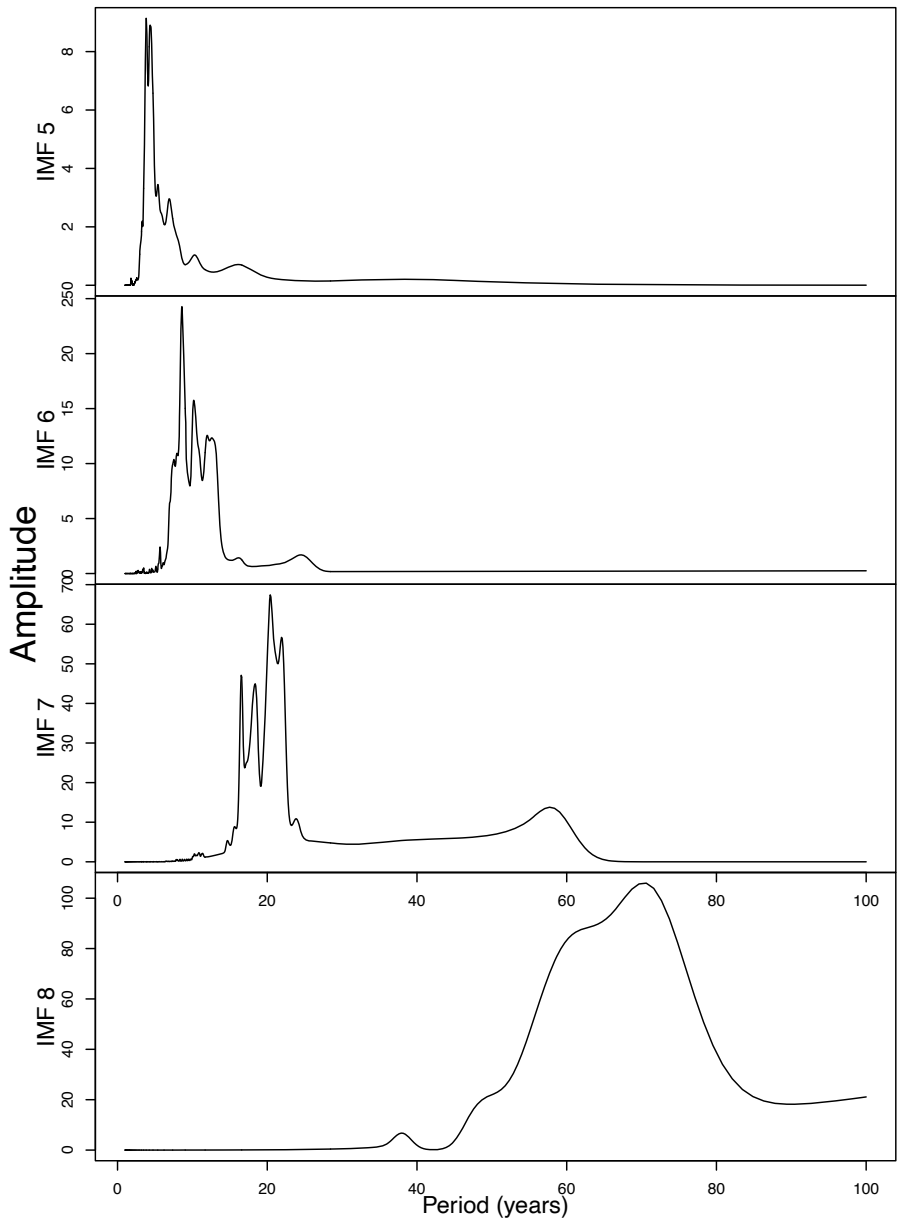

Fig. 7 Inverted Marginal Hilbert Spectra, IMFs 5-8

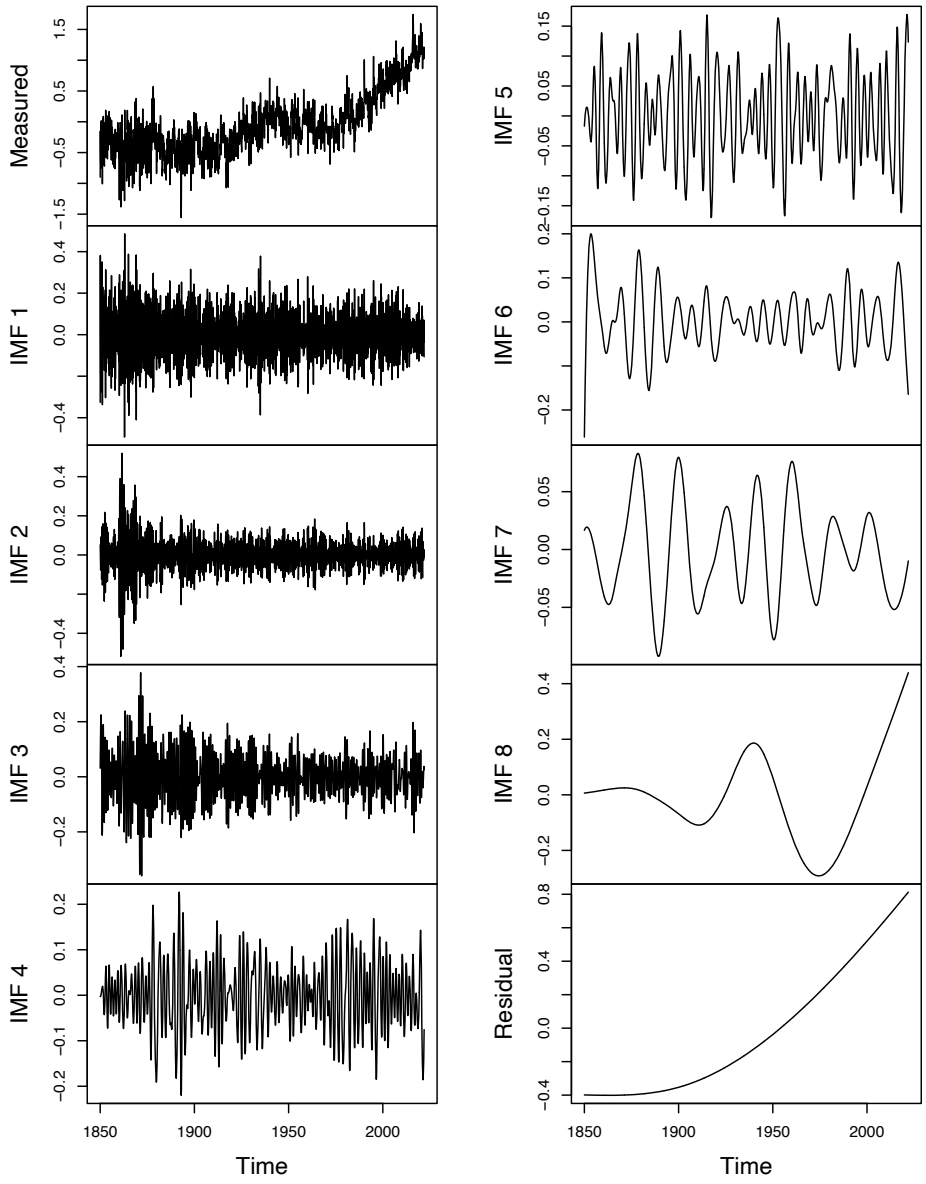

Fig. 8 Average Mean Northern Hemisphere Temperature Anomalies with ICEEMDAN Decomposition (°C), 1850-2021

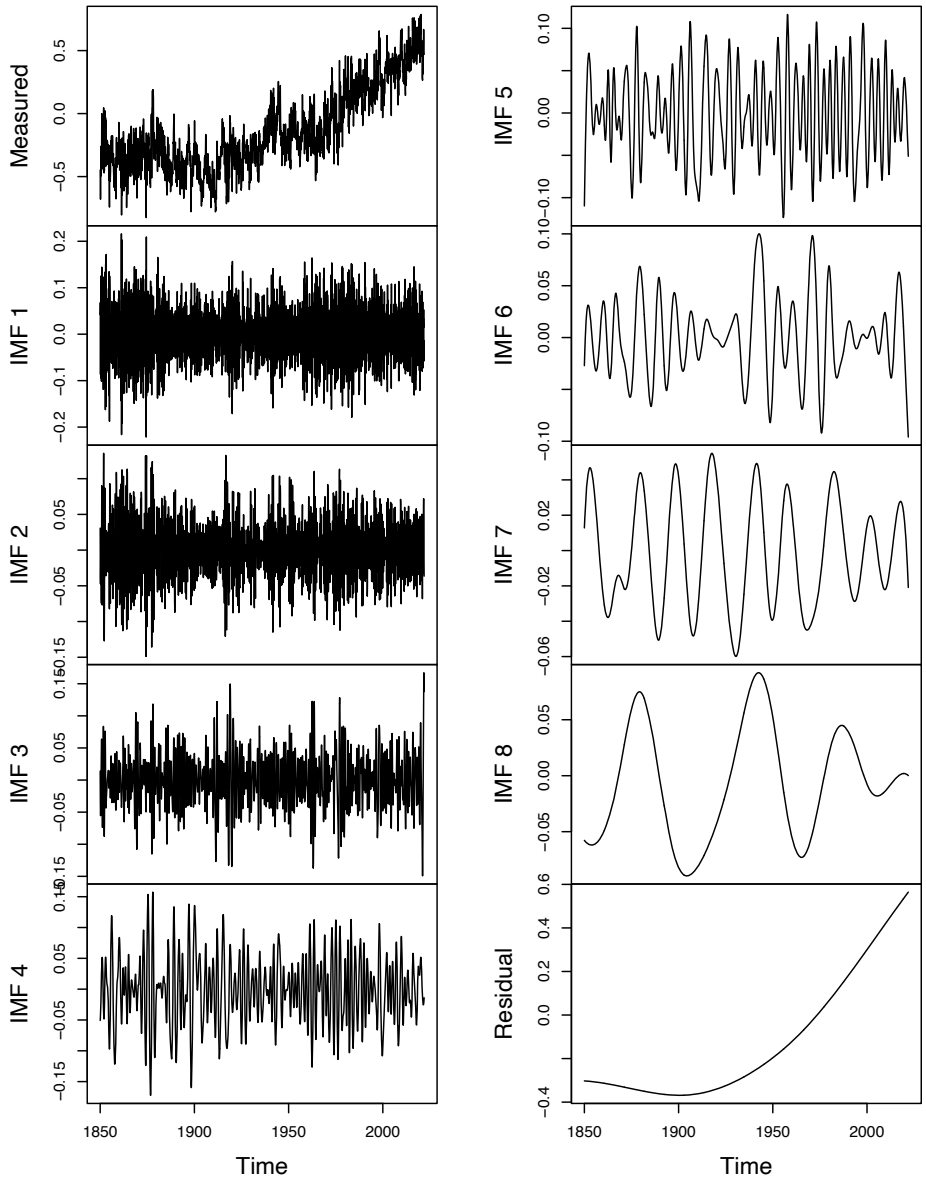

Fig. 9 Average Mean Southern Hemisphere Temperature Anomalies with ICEEMDAN Decomposition (°C), 1850-2021

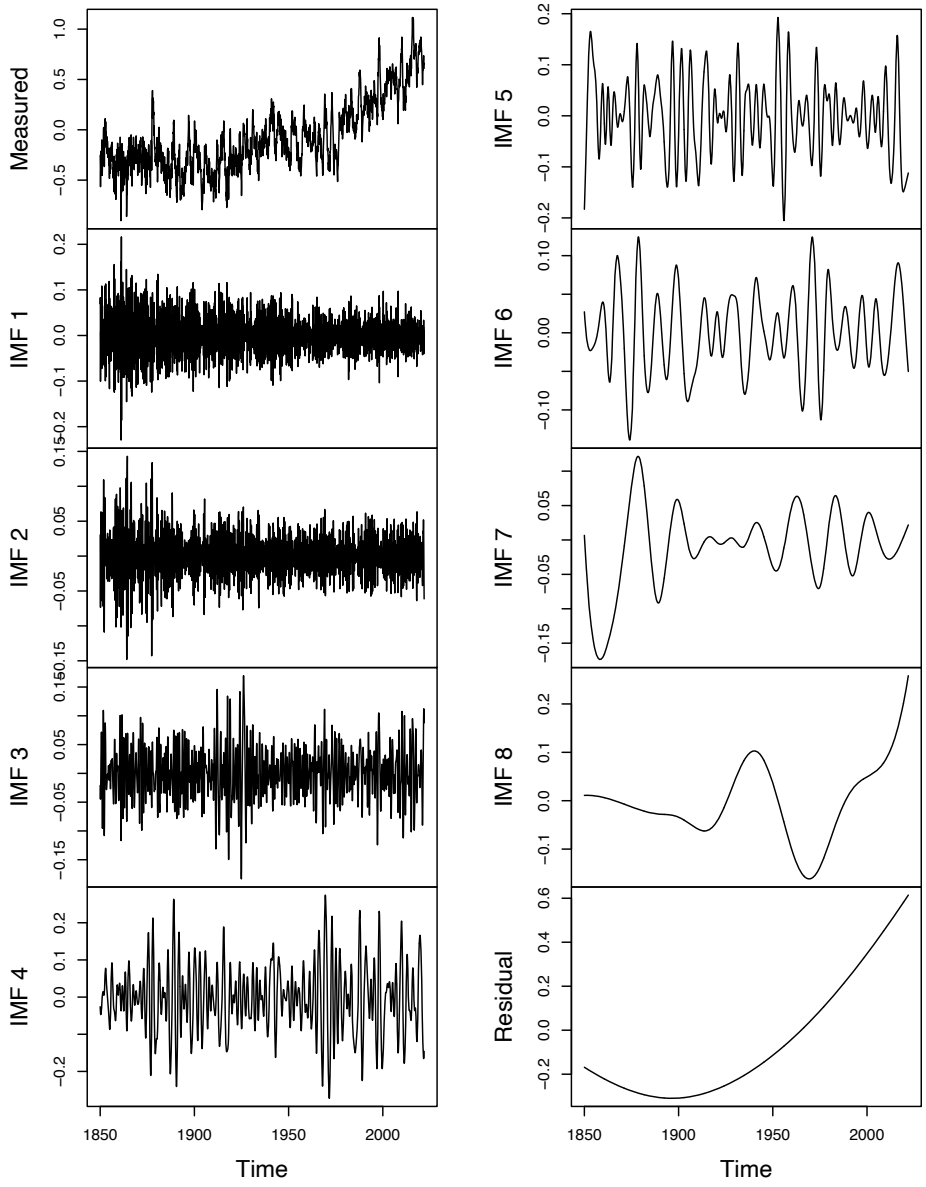

Fig. 10 Average Mean Tropical Temperature Anomalies with ICEEMDAN Decomposition (°C), 1850-2021

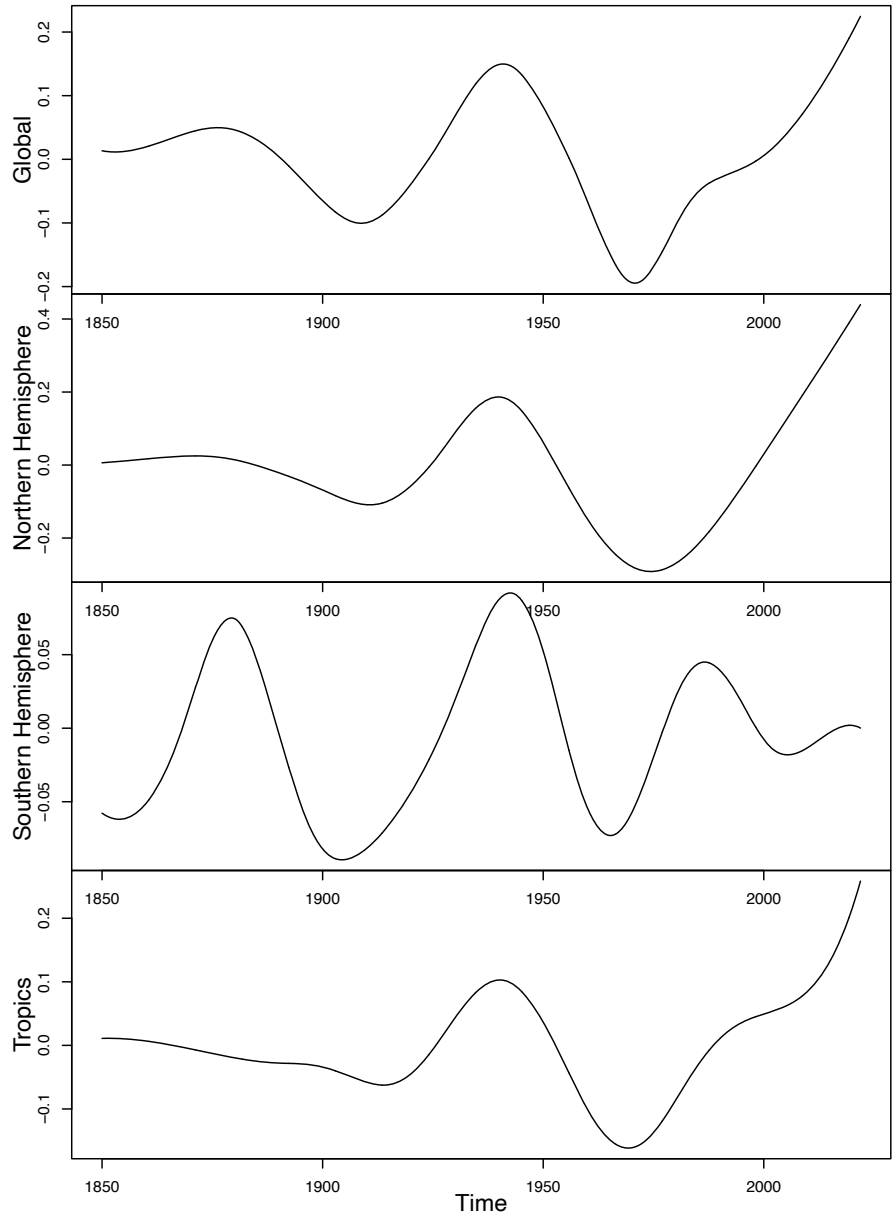

Fig. 11 IMF 8, Globally and Regionally (°C), 1850-2021

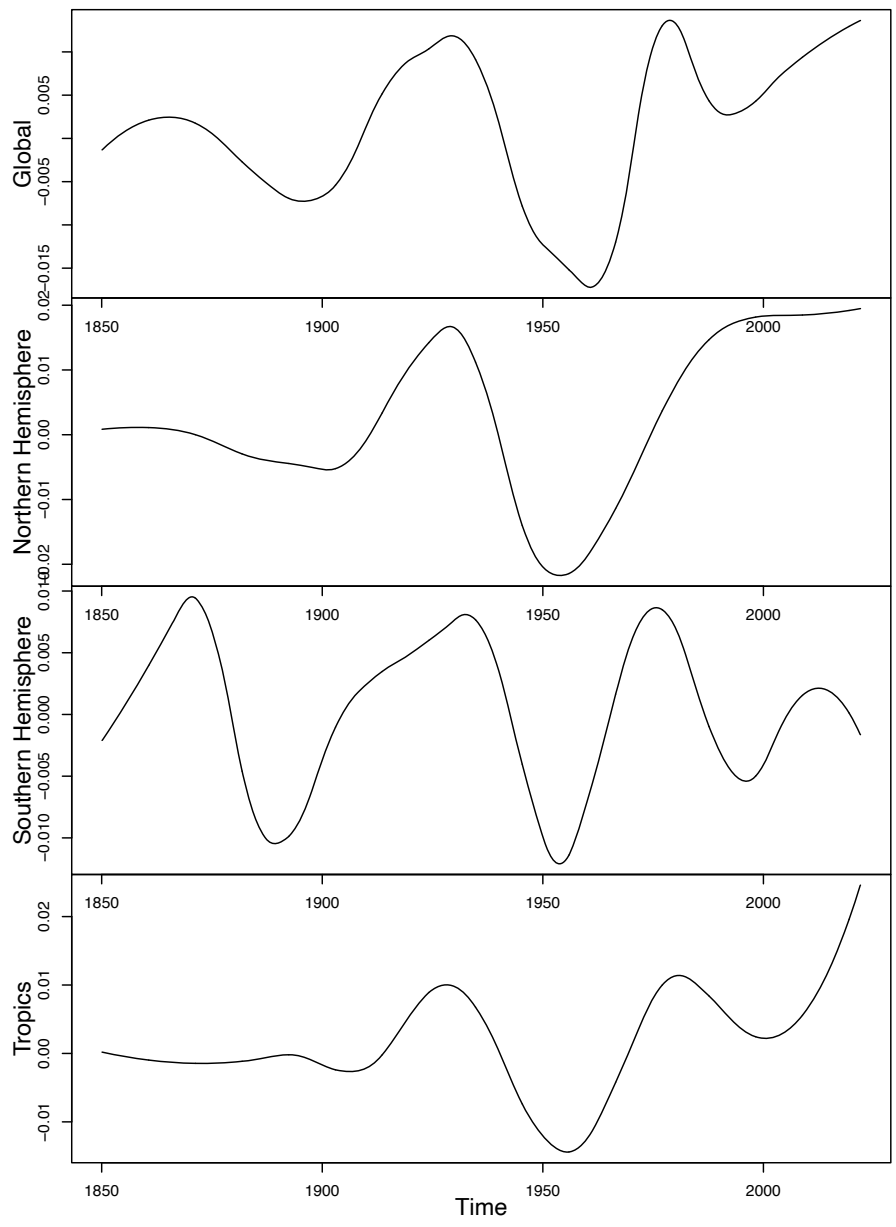

Fig. 12 First Derivative of IMF 8, Globally and Regionally (°C), 1850-2021

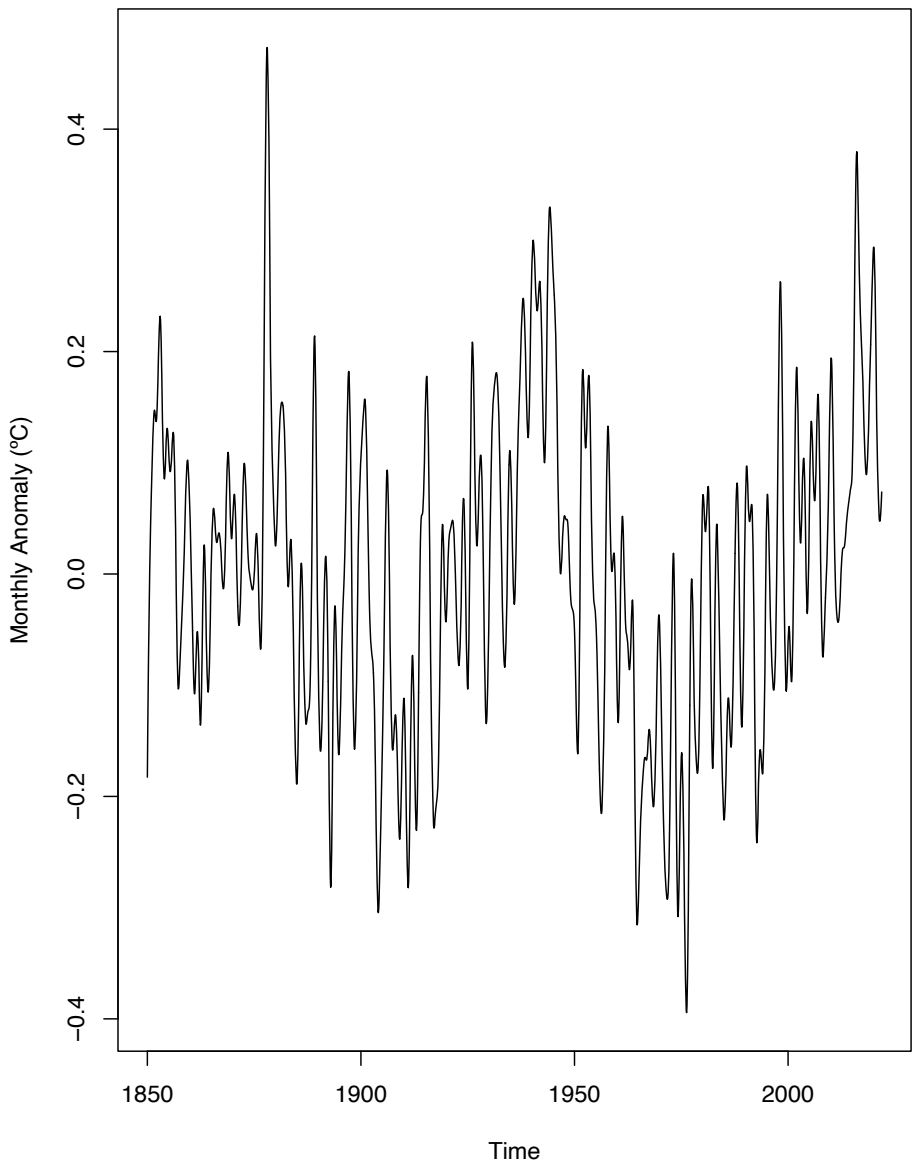

Fig. 13 Sum of Global IMFs 5-8 and Residual (°C), 1850-2021

Code availability

All programming was done in R. The R programs and workspace file are included in the supplemental materials.

Author's Contribution

The author declares that he is the sole author of this work.

Author Declarations

Not applicable.

Funding

Not applicable.

Conflict of interest

The author declares that he has no conflict of interest.

References

Björnsson H, Venegas SA (2000) A manual for EOF and SVD analyses of climate data. Tech. rep., McGill University, Móntreal, Québec, Canada, URL `http://muenchow.cms.udel.edu/classes/MAST811/eof.pdf`

Bretherton CS, Widmann M, Dymnikov VP, Wallace JM, Blade I (1999) The effective number of spatial degrees of freedom of a time-varying field. Journal of Climate 12:1990–2009

Colominas MA, Schlotthauer G, Torres ME (2014) Improved complete ensemble EMD: A suitable tool for biomedical signal processing. Biomedical Signal Processing and Control 14:19–29, DOI https://doi.org/10.1016/j.bspc.2014.06.009

Dai A, Luo D, Song M, Liu J (2019) Arctic amplification is caused by sea-ice loss under increasing CO2. Nature Communications 10(1):121, DOI https://doi.org/10.1038/s41467-018-07954-9

Deering R, Kaiser J (2005) The use of a masking signal to improve empirical mode decomposition. In: Proceedings. (ICASSP '05). IEEE International Conference on Acoustics, Speech, and Signal Processing, 2005., vol 4, pp iv/485 – iv/488 Vol. 4, DOI https://doi.org/10.1109/ICASSP.2005.1416051

Easterling DR, Wehner MF (2009) Is the climate warming or cooling? Geophysical Research Letters 36:L08706, DOI https://doi.org/10.1029/2009GL037810

Fauchereau N, Pegram G, Sinclair S (2008) Empirical mode decomposition on the sphere: application to the spatial scales of surface temperature variations. Hydrology and Earth System Sciences 12:1–9, DOI https://doi.org/10.5194/hess-12-933-2008

Feldstein SB (2002) The recent trend and variance increase of the annular mode. Journal of Climate 15:88–94

Foster G, Rahmstorf S (2011) Global temperature evolution 1979–2010. Environmental Research Letters 6(4):044022, DOI https://doi.org/10.1088/1748-9326/6/4/044022

Franzke C (2010) Long-range dependence and climate noise characteristics of antarctic temperature data. Journal of Climate 23(22):6074–6081, DOI https://doi.org/10.1175/2010jcli3654.1

Hansen J, Sato M (2021) July temperature update: Faustian payment comes due. URL `http://www.columbia.edu/~mhs119/Temperature/Emails/July2021.pdf`

Hansen J, Sato M, Ruedy R, Lo K, Lea DW, Medina-Elizade M (2006) Global temperature change. Proceedings of the National Academy of Sciences 103(39):14288–14293, DOI https://doi.org/10.1073/pnas.0606291103

Hansen J, Sato M, Ruedy R (2013) Global temperature update through 2012. URL `https://www.nasa.gov/pdf/719139main\_2012\_GISTEMP\_summary.pdf`

Huang NE, Shen Z, Long SR, Wu MC, Shih HH, Zheng Q, Yen NC, Tung CC, Liu HH (1998) The Empirical Mode Decomposition and the Hilbert spectrum for nonlinear and non-stationary time series analysis. Proceedings of the Royal Society of London A 454(1971):903–995

Huang NE, WU Z, Pinzón JE, Parkinson CL, Long SR, Blank K, Gloersen P, Chen X (2009) Reductions of noise and uncertainty in annual global surface temperature anomaly data. Advances in Adaptive Data Analysis 1(3):447–460

Hugonnet R, McNabb R, Berthier E, Menounos B, Nuth C, Girod L, Farinotti D, Huss M, Dussaillant I, Brun F, Kääb A (2021) Accelerated global glacier mass loss in the early twenty-first century. Nature 592(7856):726–731, DOI https://doi.org/10.1038/s41586-021-03436-z

Keenan TF, Prentice IC, Canadell JG, Williams CA, Wang H, Raupach M, Collatz GJ (2016) Recent pause in the growth rate of atmospheric CO2 due to enhanced terrestrial carbon uptake. Nature Communications 7(13428), DOI https://doi.org/10.1038/ncomms13428

Kim D, Kim KO, Oh HS (2012) Extending the scope of empirical mode decomposition by smoothing. Journal on Advances in Signal Processing 2012(168)

Lau KM, Weng H (1999) Interannual, decadal–interdecadal, and global warming signals in sea surface temperature during 1955–97. Journal of Climate 12(5):1257–1267, DOI https://10.1175/1520-0442(1999)012\textless1257:idiagw\textgreater2.0.co;2

Lean JL, Rind DH (2008) How natural and anthropogenic influences alter global and regional surface temperatures: 1889 to 2006. Geophysical Research Letters 35(18), DOI https://doi.org/10.1029/2008gl034864

Leggett LMW, Ball DA (2015) Granger causality from changes in level of atmospheric CO2 to global surface temperature and the El Niño–Southern Oscillation, and a candidate mechanism in global photosynthesis. Atmosphere Chemistry and Physics 15(20):11571–11592, DOI https://doi.org/10.5194/acp-15-11571-2015

Lindsey R, Dahlman L (2020) Climate change: Global temperature. URL `https://www.climate.gov/news-features/understanding-climate/climate-change-global-temperature`

Loeb NG, Johnson GC, Thorsen TJ, Lyman JM, Rose FG, Kato S (2021) Satellite and ocean data reveal marked increase in earth's heating rate. Geophysical Research Letters 48(13):e2021GL093047, DOI https://doi.org/10.1029/2021GL093047

McCloskey D, Ziliak S (2008) The Cult of Statistical Significance. University of Michigan Press, DOI https://doi.org/10.3998/mpub.186351

Morice C, Kennedy J, Rayner N, Winn J, Hogan E, Killick R, Dunn R, Osborn T, Jones P, Simpson I (in press) An updated assessment of near-surface temperature change from 1850: The HadCRUT5 dataset. Journal of Geophysical Research (Atmospheres) DOI https://doi.org/10.1029/2019JD032361

Mukherjee S, Joshi R, Prasad RC, Vishvakarma SCR, Kumar K (2014) Summer monsoon rainfall trends in the Indian Himalayan region. Theoretical and Applied Climatology 121(3-4):789–802, DOI https://doi.org/10.1007/s00704-014-1273-1

National Snow and Ice Data Center (2020) SOTC: Sea ice

Qian C (2015) On trend estimation and significance testing for non-gaussian and serially dependent data: quantifying the urbanization effect on trends in hot extremes in the megacity of shanghai. Climate Dynamics 47(1-2):329–344, DOI https://doi.org/10.1007/s00382-015-2838-0

R Core Team (2020) R: A Language and Environment for Statistical Computing. R Foundation for Statistical Computing, Vienna, Austria, URL `https://www.R-project.org/`

Ridley DA, Solomon S, Barnes JE, Burlakov VD, Deshler T, Dolgii SI, Herber AB, Nagai T, III RRN, Nevzorov AV, Ritter C, Sakai T, Santer BD, Sato M, Schmidt A, Uchino O, Vernier JP (2014) Total volcanic stratospheric aerosol optical depths and implications for global climate change. Geophysical Research Letters 41(22):7763–7769, DOI https://doi.org/10.1002/2014GL061541

Sabzehee F, Nafisi V, Iran Pour S, Vishwakarma BD (2019) Geospatial conference 2019 – joint conferences of SMPR and GI research. In: The International Archives of the Photogrammetry, Remote Sensing and Spatial Information Sciences, Analysis of the precipitational climate signal using Empirical Mode Decomposition (EMD) over the Caspian catchment area, vol XLII-4/W18, pp 923–929, DOI https://10.5194/isprs-archives-XLII-4-W18-923-2019

Shi F, Yang B, von Gunten L, Qin C, Wang Z (2011) Ensemble empirical mode decomposition for tree-ring climate reconstructions. Theoretical and Applied Climatology 109(1-2):233–243, DOI https://doi.org/10.1007/s00704-011-0576-8

Silva CB, Silva MES, Krusche N, Ambrizzi T, de Jesus Ferreira N, da Silva Dias PL (2018) The analysis of global surface temperature wavelets from 1884 to 2014. Theoretical and Applied Climatology 136(3-4):1435–1451, DOI https://doi.org/10.1007/s00704-018-2569-3

Torres ME, Colominas MA, Schlotthauer G, Flandrin P (2011) A complete ensemble empirical mode decomposition with adaptive noise. In: 2011 IEEE International Conference on Acoustics, Speech and Signal Processing (ICASSP), pp 4144–4147

Turner J, Colwell SR, Marshall GJ, Lachlan-Cope TA, Carleton AM, Jones PD, Lagun V, Reid PA, Iagovkina S (2005) Antarctic climate change during the last 50 years. International Journal of Climatology 25(3):279–294, DOI https://doi.org/10.1002/joc.1130

Wang H, Mehta VM (2008) Decadal variability of the Indo-Pacific warm pool and its association with atmospheric and oceanic variability in the NCEP-NCAR and SODA reanalyses. Journal of Climate 21(21):5545–5565, DOI https://doi.org/10.1175/2008jcli2049.1

Wu Z, Huang N (2009) Ensemble empirical mode decomposition: a noise-assisted data analysis method. Advances in Adaptive Data Analysis 1:1–41, DOI https://doi.org/10.1142/S1793536909000047

Wu Z, Huang NE, Wallace JM, Smoliak BV, Chen X (2011) On the time-varying trend in global-mean surface temperature. Climate Dynamics 37(3-4):759–773, DOI https://doi.org/10.1007/s00382-011-1128-8

Xing P, Chen X, Luo Y, Nie S, Zhao Z, Huang J, Wang S (2016) The extratropical northern hemisphere temperature reconstruction during the last millennium based on a novel

method. PLOS ONE 11(1):e0146776, DOI https://doi.org/10.1371/journal.pone.0146776

Yang C, Wu H, Hu D (2011) Relationship between air temperature oscillations and solar variability on short and medium time scales. Science China Earth Sciences 54(6):912–923, DOI https://doi.org/10.1007/s11430-010-4161-2

Yang P, Wang G, Zhang F, Zhou X (2015) Causality of global warming seen from observations: a scale analysis of driving force of the surface air temperature time series in the northern hemisphere. Climate Dynamics 46(9-10):3197–3204, DOI https://doi.org/10.1007/s00382-015-2761-4

Zhou J, Tung KK (2013) Deducing multidecadal anthropogenic global warming trends using multiple regression analysis. Journal of the Atmospheric Sciences 70(1):3–8, DOI https://doi.org/10.1175/jas-d-12-0208.1

Ziliak ST, McClosskey DN (2004) The standard error of regressions in the *american economic review*. Journal of Socio-Economics 33(5):527–546, DOI https://doi.org/10.1016/j.socec.2004.09.024

Supplementary Files

This is a list of supplementary files associated with this preprint. Click to download.

- 5
- IMFdemod.r
- calcIMF8skewness.r
- calcenergies.r
- calctrendchanges.r
- extractfinalimfstemp.r
- extractfinalspectratemps.r
- iceemdan.r
- iceemdanP.r
- mhs.r
- printgraphs.r
- processtemperature.r
- processtemperaturenh.r
- processtemperaturesh.r
- processtemperaturetropics.r